Nuclear Instruments and Methods in Physics Research A 664 (2012) 49–64

Contents lists available at SciVerse ScienceDirect

Nuclear Instruments and Methods in Physics Research A

journal homepage: www.elsevier.com/locate/nima

Correcting systematic errors in high-sensitivity deuteron polarization measurements

N.P.M. Brantjes [a], V. Dzordzhadze [b], R. Gebel [c], F. Gonnella [d,e], F.E. Gray [f], D.J. van der Hoek [a], A. Imig [b], W.L. Kruithof [a], D.M. Lazarus [b], A. Lehrach [c], B. Lorentz [c], R. Messi [d,e], D. Moricciani [e], W.M. Morse [b], G.A. Noid [g], C.J.G. Onderwater [a], C.S. Özben [h], D. Prasuhn [c], P. Levi Sandri [i], Y.K. Semertzidis [b], M. da Silva e Silva [a], E.J. Stephenson [g,*], H. Stockhorst [c], G. Venanzoni [i], O.O. Versolato [a]

[a] Kernfysisch Versneller Instituut, University of Groningen, NL-9747AA Groningen, The Netherlands
[b] Brookhaven National Laboratory, Upton, NY 11973, USA
[c] Institut für Kernphysik, Jülich Center for Hadron Physics, Forschungszentrum Jülich, D-52425 Jülich, Germany
[d] Physica Department of "Tor Vergata" University, Rome, Italy
[e] INFN-Sez. "Roma tor Vergata," Rome, Italy
[f] Regis University, Denver, CO 80221, USA
[g] Indiana University Cyclotron Facility, Bloomington, IN 47408, USA
[h] Istanbul Technical University, Instanbul 34469, Turkey
[i] Laboratori Nazionali di Frascati dell'INFN, Frascati, Italy

ARTICLE INFO

Article history:
Received 8 May 2011
Received in revised form
15 September 2011
Accepted 20 September 2011
Available online 20 October 2011

Keywords:
Electric dipole moment
Polarimeter
Deuteron
Storage ring

ABSTRACT

This paper reports deuteron vector and tensor beam polarization measurements taken to investigate the systematic variations due to geometric beam misalignments and high data rates. The experiments used the In-Beam Polarimeter at the KVI-Groningen and the EDDA detector at the Cooler Synchrotron COSY at Jülich. By measuring with very high statistical precision, the contributions that are second-order in the systematic errors become apparent. By calibrating the sensitivity of the polarimeter to such errors, it becomes possible to obtain information from the raw count rate values on the size of the errors and to use this information to correct the polarization measurements. During the experiment, it was possible to demonstrate that corrections were satisfactory at the level of 10^{-5} for deliberately large errors. This may facilitate the real time observation of vector polarization changes smaller than 10^{-6} in a search for an electric dipole moment using a storage ring.

1. Introduction

It has been proposed [1] that a storage ring can be used to search for an intrinsic electric dipole moment (EDM) that might be present on the charged particles in a polarized beam, thus opening such searches to non-neutral systems. The sensitivity level could approach 10^{-29} e cm per year of observation. Any intrinsic electric dipole moment would be aligned along the particle spin axis. The combination of the vector electric dipole with the pseudo-vector spin makes such a combination a violation of both parity conservation and time reversal invariance. Any observation of a non-vanishing EDM at the level of 10^{-29} e cm would be larger than any effect predicted to come from the Standard Model and thus it would be a signature of a new, CP-violating physical process. Such a process is needed to explain the excess abundance of matter over anti-matter in the universe.

For the stored, polarized beam, one effect of an EDM is the precession of the polarization from the longitudinal into the vertical direction in the presence of a strong radial electric field. Making such an observation requires a scheme for maintaining the beam polarization along the direction of the beam velocity in spite of forces that would normally rotate the spin in the storage ring plane and random effects that would cause the spin directions of the beam particles to decohere. By making the observed polarization component vertical, the EDM signal itself is free of these two effects and stable enough for measurement in a beam polarimeter.

For the proton with its large, positive anomalous magnetic moment, circulation of the beam in an all-electric ring at a momentum of about $p=0.701$ GeV/c makes the rotation of the proton spin match the rotation of the velocity. The spin rotation comes from the effective magnetic field (equal to $-\gamma\mathbf{v}\times\mathbf{E}$) that appears in the proton frame from the radial electric field that holds the proton in orbit around the ring. For the deuteron case with a small, negative anomalous magnetic moment, the magnetic storage

* Corresponding author. Tel.: +1 812 855 5469; fax: +1 812 855 6645.
E-mail address: stephene@indiana.edu (E.J. Stephenson).

0168-9002/$ - see front matter © 2011 Elsevier B.V. All rights reserved.
doi:10.1016/j.nima.2011.09.055

ring requires the addition of an outward, radial electric field to increase the ring circumference until the spin and velocity rotations synchronize. In this case, the electric field that acts on the EDM comes mostly from the effective electric field ($\gamma\mathbf{v}\times\mathbf{B}$) in the deuteron frame generated by the ring magnets. In both cases, the ring lattice, including components up through sextupole terms, must be designed to minimize the spread of particle spin directions due to betatron oscillations and different particle momenta.

A storage ring experiment to search for an EDM requires the measurement of a change in the vertical polarization component that is consistent with the time integral of the longitudinal beam polarization, which may be depolarizing during the beam storage time of about 1000 s. A sensitivity of 10^{-29} e cm with an upper limit of 2×10^{11} on the number of stored particles due to collective effects requires ring operation for most of a year with a beam polarimeter having an analyzing power of at least 0.5. The polarimeter efficiency must be high enough that up to 1% of the particles extracted onto the polarimeter target scatter into the detectors and can be used to determine either horizontal or vertical asymmetries. The horizontal asymmetry is sensitive to the vertical polarization component and thus to the EDM; the vertical asymmetry monitors the longitudinal alignment of the polarization by verifying that the sideways polarization component is minimal. The longitudinal component itself becomes observable when a small breaking of the matching conditions described above allows the polarization to rotate in the horizontal plane away from the beam direction. The EDM signal associated with a 10^{-29} e cm sensitivity is a rotation in the polarization of a few micro-radians for deuterium. Thus it is also important that systematic errors in the polarimeter are reduced below the level of 10^{-6} even with changing beam current and variations in beam position and angle.

This paper reports the results of successful experiments to demonstrate that the required efficiency can be obtained with thick carbon extraction targets located close to the beam. Also, the systematic polarization errors can be corrected in real time to below the 10^{-5} level based on a prior calibration of the polarimeter and independent measures of the size of any systematic error sources. These techniques are more generally applicable and may prove useful for the measurement of the small asymmetries that often arise in studies of parity or time reversal violation. These techniques do not address the independent question of how to measure a sizable polarization effect with great precision.

Most of this paper is devoted to the treatment of systematic errors in polarization measurements. The results concerning the efficiency of the polarimeter are discussed in Section 3.3. In all cases, a polarized deuteron beam is used. This allows for the inclusion of tensor asymmetries in the treatment of polarization observables.

While in principle it is possible to measure a vector beam polarization merely by observing the change that it creates in the cross section for some reaction or scattering process; there are two methods that are in common use to reduce systematic errors. One is the placement of identical detectors on both sides of the beam (horizontally left and right for vector polarization along the vertical axis); the polarization effects are opposite and the measurement reduces to the observation of an asymmetry (difference divided by the sum of the rates). Another is the repetition of the experiment with the direction of the polarization reversed, an action that swaps the changes between left and right. Both techniques can be used together, yielding four independent measurements of the counting rate that can be combined to give the asymmetry (product of the polarization and analyzing power) in a way, sometimes called the "cross ratio," that nominally cancels problems with the relative intensity of the two polarized beam states and acceptance differences between the two detectors [2].

The cross ratio cancels a number of other systematic errors, such as a beam misalignment, at first order (linear) in the error. Section 2 contains a demonstration that it fails at second order (quadratic and higher), creating a problem for experiments that require high sensitivity to small polarizations. This demonstration compares data from the Kernfysisch Versneller Instituut at the University of Groningen with an analytic derivation of second-order effects and a prediction based on a separately-measured angular distribution of the vector analyzing power.

Section 3 introduces two different combinations of the four cross ratio count rates described above that are sensitive to the presence of a geometrical misalignment or changes in the data acquisition rate while at the same time being relatively insensitive to the polarization. These combinations become the driving terms for a scheme to correct the polarization for systematic errors, provided that the polarimeter has been previously calibrated for its systematic error sensitivity. This calibration introduces controlled errors that are much larger than any that would be encountered during a real experiment and measures their effects on any polarization observables. This scheme was successfully tested during an experiment at the Cooler Synchrotron COSY [3] located at the Forschungszentrum Jülich. In addition, these tests demonstrated that a correction based on the geometric driving term worked equally well for beam position and angle errors. In order to build confidence in the correction scheme, a model was created with a variety of ways whereby geometric and counting rate errors could alter a polarization measurement. These ways were all independently calibrated using the COSY measurements, and it was found that this model was sufficient to explain the COSY data.

Thus it is possible to correct the cross ratio asymmetry using an expression that contains systematic error calibration information and the four cross ratio counting rates. This scheme can be used in real time to generate polarization measurements corrected for systematic errors present at the time of the measurement. Other polarization observables such as first-order or tensor asymmetries yield to a similar treatment and are also correctable.

2. Initial investigation of second-order contributions to systematic polarization errors

2.1. The parameterization of geometric errors in the polarization

The differential cross section for a polarized spin-1 beam with a quantization axis perpendicular to the beam may be written in Cartesian notation as

$$\sigma_{POL}(\Theta)=\sigma_{UNPOL}(\Theta)[1+2it_{11}iT_{11}(\Theta)+t_{20}T_{20}(\Theta)+2t_{22}T_{22}(\Theta)] \quad (1)$$

where Θ is the scattering angle measured from the direction of the beam velocity toward the detector. In this expression and the subsequent ones, σ represents the differential cross section often written as $d\sigma/d\Omega$. The derivative notation is reserved here to describe changes to this cross section from changes in the angle of the beam on target. The t_i represent polarizations, and the T_i represent analyzing powers, which, like the cross sections, are functions of the scattering angle.

In a typical polarized ion source with a magnetically-imposed quantization axis, the vector (V) and tensor (T) polarizations are given by the fractions of the beam that are in each of the spin-1 magnetic substates, f_1, f_0, and f_{-1}, as

$$p_V=f_1-f_{-1} \quad \text{and} \quad p_T=1-3f_0. \quad (2)$$

If the quantization axis lies in the X–Y plane perpendicular to the beam, its direction may be described by an angle ψ. This direction corresponds to the direction of the spin in the $m=1$

magnetic substate. The angle is zero when the quantization axis points along the vertical (Y) axis. The angle increases from zero as the quantization axis moves away from the Y-axis and toward the horizontal (X) axis, which points in the scattering plane on the side toward the detector. The polarizations of Eq. (1) are given by

$$it_{11}=\frac{\sqrt{3}}{2}p_V\cos\psi,\quad t_{20}=-\frac{1}{2\sqrt{2}}p_T,\quad \text{and}\quad t_{22}=-\frac{\sqrt{3}}{4}p_T\cos 2\psi. \tag{3}$$

For the EDM search, the large vector analyzing powers available with suitably chosen targets make it preferable to concentrate on this polarization measurement rather than the tensor. Even so, the asymmetry from the tensor polarization will be considered in the analysis of geometric effects discussed in this paper. It may ultimately prove useful for monitoring the performance of an EDM search.

This section continues with a discussion of geometric systematic errors in the measurement of vector polarization. For clarity, we will use a simplified notation. The polarized differential cross section on beam left (σ_L) is described in as

$$\sigma_L=\sigma_{UNP}(1+pA) \tag{4}$$

where σ_{UNP} denotes the unpolarized differential cross section, $p=it_{11}$ the polarization, and $A=2iT_{11}(\Theta)$ the deuteron analyzing power. The product $\varepsilon=pA$ is called the asymmetry because the $\cos\psi$ dependence of Eq. (3) creates opposite changes on the left and right sides of the beam, making previously symmetric rates asymmetric.

In a polarimeter with a large detector acceptance (as is needed for high statistics and sensitivity to small polarizations) the unpolarized cross section and analyzing power become average quantities over the acceptance solid angle. To parameterize geometric errors, it is necessary to determine how these average quantities change with small geometry changes.

Fig. 1 shows a left–right symmetric detector geometry. The beam (solid line) as it goes from left to right intercepts the target with an angular error $\Delta\theta$ that will be taken positive for the beam moving away from the left detector downstream of the target. This error is small and can be used in a Taylor series expansion of the average cross section and analyzing power:

$$\sigma_{UNP}(\Delta\theta)=\sigma_{UNP}(\Delta\theta=0)+\frac{\partial\sigma}{\partial\theta}\Delta\theta+\frac{1}{2}\frac{\partial^2\sigma}{\partial\theta^2}(\Delta\theta)^2+\cdots \tag{5}$$

$$A(\Delta\theta)=A(\Delta\theta=0)+\frac{\partial A}{\partial\theta}\Delta\theta+\frac{1}{2}\frac{\partial^2 A}{\partial\theta^2}(\Delta\theta)^2+\cdots \tag{6}$$

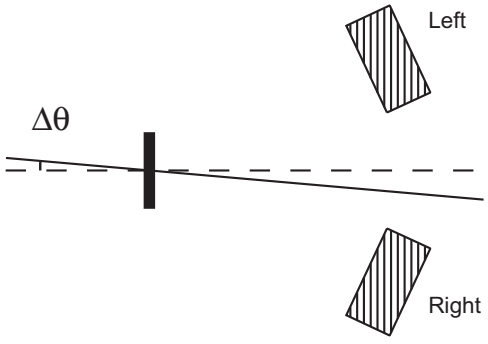

Fig. 1. Layout of an asymmetry experiment showing large area detectors as hashed rectangles at the same scattering angle on the left and right sides of the beam. The beam centerline runs through the target along the dashed line and bisects the detector geometry. The actual beam (solid line) intercepts the center of the target but at an angle error $\Delta\theta$ that is positive for increasing scattering angles on the left side.

A position error may be treated in a similar fashion except that it is also necessary to consider the effects of a change of solid angle on the detector rate, and this introduces additional terms into the expansion. The discussion later will cover the relationship between these two types of errors for the sort of forward detector geometry planned for the EDM search. The derivatives such as $\partial\sigma/\partial\theta$ are the properties of the polarimeter detector system and represent the size of any effect on the cross section or analyzing power produced by a particular error. It is these derivatives that must be determined during a systematic error calibration.

The derivatives may also be estimated if the measurements of an angular distribution are available. In that case, the measurements are a function of the scattering angle Θ so that

$$\frac{\partial\sigma}{\partial\theta}=\frac{\partial}{\partial\Theta}\int_{acc}\frac{\partial\sigma(\Omega)}{\partial\Omega}\,d\Omega \tag{7}$$

and the integral runs over the acceptance (solid angle) subtended by the detectors.

If the left–right asymmetry is measured, the angular error modifies the asymmetry according to

$$\varepsilon(\Delta\theta)=\frac{\sigma_L-\sigma_R}{\sigma_L+\sigma_R}=\varepsilon(\Delta\theta=0)+\left[\frac{1}{\sigma}\frac{\partial\sigma}{\partial\theta}-\varepsilon^2\left(\frac{1}{\sigma}\frac{\partial\sigma}{\partial\theta}+\frac{1}{A}\frac{\partial A}{\partial\theta}\right)\right]\Delta\theta+\left\{\varepsilon\left[\frac{1}{2A}\frac{\partial^2 A}{\partial\theta^2}-\left(\frac{1}{\sigma}\frac{\partial\sigma}{\partial\theta}\right)^2\right]+\varepsilon^3\left(\frac{1}{\sigma}\frac{\partial\sigma}{\partial\theta}+\frac{1}{A}\frac{\partial A}{\partial\theta}\right)^2\right\}(\Delta\theta)^2 \tag{8}$$

where the correct asymmetry is $\varepsilon=\varepsilon(\Delta\theta=0)$ and both first- and second-order changes appear due to the error $\Delta\theta$. It should be noted that for small asymmetries the first-order term is dominated by the logarithmic derivative of the cross section. This is the only term that does not scale with some power of the asymmetry. For sensitive measurements this term can easily exceed the size of any signal of interest. The asymmetry is used to extract the beam polarization through $p=\varepsilon/A$.

The cross ratio method [2] for obtaining the asymmetry involves the use of two polarization states with opposite signs of the polarization p_V, denoted as $(+)$ and $(-)$ in

$$\varepsilon_{CR}=\frac{r-1}{r+1}$$

where

$$r^2=\frac{\sigma_L(+)\sigma_R(-)}{\sigma_L(-)\sigma_R(+)}. \tag{9}$$

In this case, there is one more "small" error parameter that is needed, the difference in the magnitudes of the $(+)$ and $(-)$ polarizations. Here that is denoted by u so that the spin up polarization is $p(+)=u+p$ and $p(-)=u-p$ with p the average polarization magnitude and $2u$ the difference in magnitudes. An angular error then produces a change in the cross ratio asymmetry of

$$\varepsilon_{CR}(\Delta\theta)=\varepsilon_{CR}(\Delta\theta=0)+\frac{\varepsilon^2}{1-\varepsilon^2}u^2-\frac{2\varepsilon^2}{1-\varepsilon^2}\frac{1}{A}\frac{\partial A}{\partial\theta}u(\Delta\theta)+\left[\frac{\varepsilon}{2}\frac{1}{A}\frac{\partial^2 A}{\partial\theta^2}-\frac{\varepsilon^2}{1-\varepsilon^2}\left(\frac{1}{A}\frac{\partial A}{\partial\theta}\right)^2\right](\Delta\theta)^2. \tag{10}$$

In this case there are no first-order error terms and there are no derivatives of the cross section. This makes the error contributions to the cross ratio asymmetry small and favors the use of the cross ratio in polarization experiments.

In practice, there are other schemes that are sometimes employed to cancel the systematic error contributions to the asymmetry. One involves the subtraction of the asymmetry measured with an unpolarized beam. In this case

$$\varepsilon_{SUB}=\frac{\sigma_L-\sigma_R}{\sigma_L+\sigma_R}-\frac{\sigma_L-\sigma_R}{\sigma_L+\sigma_R}(p=0) \tag{11}$$

and the systematic error contributions are

$$\varepsilon_{SUB}(\Delta\theta)=\varepsilon_{SUB}(\Delta\theta=0)-\varepsilon^2\left(\frac{1}{\sigma}\frac{\partial\sigma}{\partial\theta}+\frac{1}{A}\frac{\partial A}{\partial\theta}\right)\Delta\theta + \left\{\varepsilon\left[\frac{1}{2A}\frac{\partial^2 A}{\partial\theta^2}-\left(\frac{1}{\sigma}\frac{\partial\sigma}{\partial\theta}\right)^2\right]+\varepsilon^3\left(\frac{1}{\sigma}\frac{\partial\sigma}{\partial\theta}+\frac{1}{A}\frac{\partial\sigma}{\partial\theta}\right)^2\right\}(\Delta\theta)^2. \quad (12)$$

In contrast to Eq. (10), this expression for the systematic error has a first-order error term that contains the logarithmic derivative of the cross section, which is often large.

In cases where there is only one vector polarized state or the difference in magnitudes (u) is particularly large, it may prove advantageous to use a "half cross ratio" formulation:

$$\varepsilon_{HCR}=\frac{r-1}{r+1} \quad \text{with} \quad r=\frac{\sigma_L(+)\sigma_R(0)}{\sigma_R(+)\sigma_L(0)} \quad (13)$$

where the comparison is between the count rates measured with a polarized and an unpolarized beam. In this case the sensitivity to an angle error is

$$\varepsilon_{HCR}(\Delta\theta)=\varepsilon_{HCR}(\Delta\theta=0)-\varepsilon^2\frac{1}{A}\frac{\partial A}{\partial\theta}\Delta\theta + \left[\varepsilon\frac{1}{2A}\frac{\partial^2 A}{\partial\theta^2}+\varepsilon^3\left(\frac{1}{A}\frac{\partial A}{\partial\theta}\right)^2\right](\Delta\theta)^2. \quad (14)$$

This expression resembles Eq. (12) with both first- and second-order terms, but the logarithmic derivative of the cross section is not present. Thus this is a preferable way to determine the asymmetry from a combination of polarized and unpolarized measurements.

The next section contains a description of the experiment designed to observe second-order systematic errors using high precision cross ratio asymmetry measurements.

2.2. Demonstration of second-order effects at the KVI

To investigate second-order systematic errors in a polarimeter, the polarized deuteron beam from the AGOR cyclotron [4] was sent at 110 MeV through the In-Beam Polarimeter (IBP) [5]. Phoswich [5] detectors consisting of a thin (2 mm), fast scintillator followed by a thick, slow scintillator served to record charged-particle events and to provide information useful for particle identification. These detectors, which were 50-mm diameter cylinders, were located at laboratory angles of 18°, 28°, 38°, and 48°. Each subtended an angle range of $\pm 2.3°$ in the laboratory. There were four sets of four detectors mounted in the left, up, right, and down directions from the target. The detector mounting arrangement is shown in Fig. 2 of Ref. [5].

When operated as a polarimeter, the target was CH_2 with a thickness of 9.8 mg/cm^2. Protons in each 38° detector were observed in coincidence with deuterons in the opposite-side 28° detector. This combination corresponded to an average center-of-mass scattering angle of 102.5°. At this angle, the IBP analyzing powers were determined from a smooth trend in energy and angle through published $d+p$ scattering data [6–9] to be $iT_{11}=-0.411\pm0.024$, $T_{20}=-0.290\pm0.033$, and $T_{22}=-0.123\pm0.004$. In the analysis, cuts were placed on the combination of fast and slow scintillator signals in order to select $d+p$ elastic scattering and to discriminate against background from deuteron breakup events. The vector beam polarization was $it_{11}=0.391\pm0.023$ for the positive vector polarized state and $it_{11}=-0.343\pm0.020$ for the negative state. The errors include the uncertainty in the calibration scale.

When operated as a test of the EDM polarimeter configuration, each Phoswich detector was run in singles mode, i.e., all events above threshold were recorded in scalers gated by the polarization state of the beam. In order to restrict the data set to particles with a higher (nearly elastic) energy, 15 mm thick aluminum absorbers were placed in front of each Phoswich detector. A carbon target of thickness 56 mg/cm^2 was cut into a strip 1 mm wide and mounted vertically. Systematic errors were produced by shifting the target to the left or right in steps of 2.5 mm. In each case, steering magnets upstream of the target were changed so that the beam through the target was maximized and only the displacement (and not the angle) of the beam was changed.

Figs. 2 and 3 show some results from this experiment; a more detailed numerical analysis is presented in the next section. Fig. 2 shows two sets of left–right asymmetry measurements (see Eq. (8))

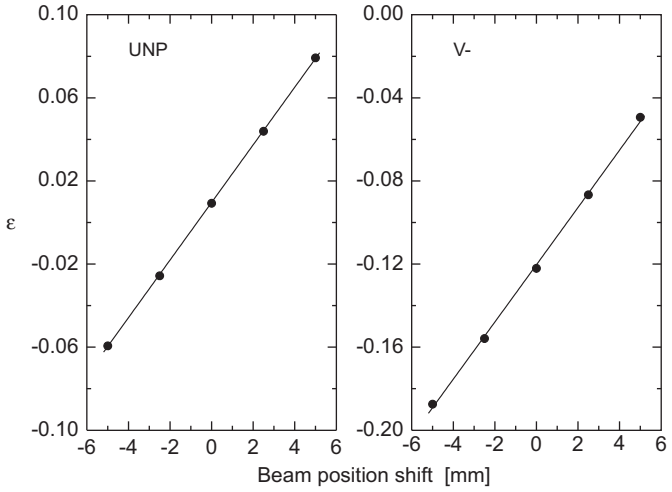

Fig. 2. Left–right asymmetries (see Eq. (8)) at a laboratory angle of 18° as a function of beam and target displacement in millimeters for the unpolarized (UNP) and negative vector (V−) polarized states. The errors are smaller than the symbols. The curves are best fit straight lines through each data set.

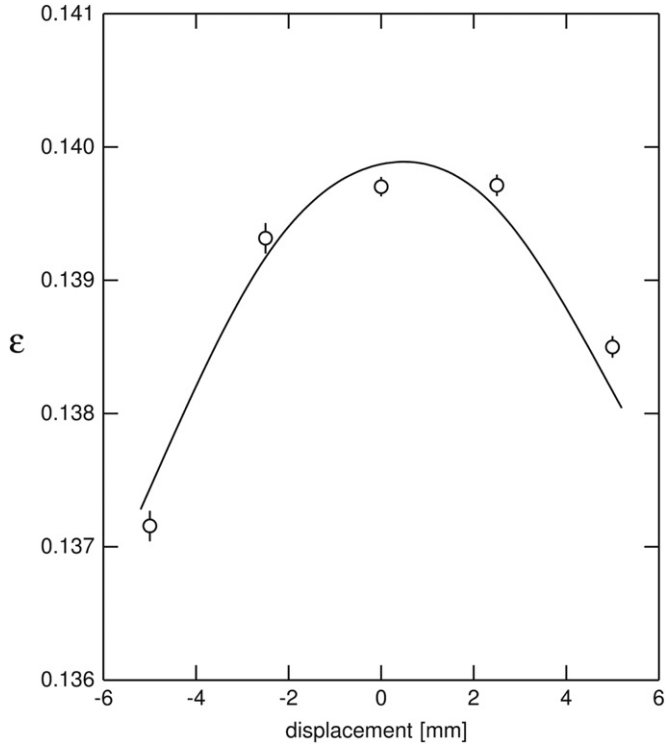

Fig. 3. Cross ratio asymmetry (see Eq. (9)) at a laboratory angle of 18° as a function of beam displacement in millimeters. The linear and quadratic contributions were calculated from a systematic error model based on elastic scattering measurements. The vertical offset of the curve was chosen arbitrarily to agree with the data.

taken at 18°. The left panel shows data for the unpolarized state and the right panel for the negative vector polarized state. Both sets of data are essentially straight lines, indicating that the dominant effect of the displacement on the asymmetry comes from the term in Eq. (8) that is linear in $\Delta\theta$ and depends on the logarithmic derivative of the cross section.

Fig. 3 shows the cross ratio based on Eq. (9). The variation with position shift is reduced by almost an order of magnitude. The dominant error term appears to be quadratic with some linear slope.

The size of the combinations of derivatives that govern the systematic error effects at each order (see Eqs. (8) and (10)) can be obtained by reproducing the effects seen in Figs. 2 and 3 with a polynomial. The next section contains a comparison of these results with predictions based on measurements of deuteron elastic scattering from carbon.

2.3. Polarimeter derivative values determined from elastic deuteron scattering

Measurements of deuteron-induced reactions on carbon were made at the KVI on two separate occasions. The first of these made use of the In-Beam Polarimeter except that the Phoswich detectors were removed for scattering to the left and right and were replaced by $\Delta E-E$ telescopes consisting of a front plastic scintillation detector 0.64-cm thick and a NaI detector (with the equivalent of a 1-mm thick aluminum can surrounding it) thick enough to stop all particles of interest. This change improved the quality of the particle identification. The left and right telescopes were placed on separate, movable stands for the purpose of measuring the angular distribution between the laboratory angles of 18° and 60°. Data were taken at 76 and 113 MeV, but only the 113-MeV measurement will be considered here. The data acquisition system was the same as that used for the IBP, except with these new detectors replacing their respective Phoswich detectors for coincident event triggering. The purpose of using a detector telescope arrangement was to provide data on scattering and reactions leading to continuum final states of as high an excitation as was reasonably practical. Carbon and polyethylene targets were used in a manner similar to that described in the previous section. The carbon target for the deuteron-induced reactions was 11.0 mg/cm^2 thick. In these data, the events originating from elastic scattering were clearly separable, as was scattering to the excited state of ^{12}C at 4.44 MeV. Measurements with these two states were obtained separately.

The second experiment made use of the Big Bite Spectrometer (BBS) located downstream of the IBP [10]. This spectrometer was used to observe particles originating from a target located on a ladder in the scattering chamber with movable vacuum seals. Scattered particles were focused by a pair of quadrupole magnets before momentum analysis was made in a large dipole magnet. Vertical-drift wire chambers located along the nominal focal plane were used to measure the position of scattered particles that continued through the chambers and into a series of plastic trigger scintillators. Data measured with the BBS were intended to extend the cross section and analyzing powers for elastic scattering into the angular region smaller than 18°. Data between the laboratory angles of 11° and 25° were collected, but only those data at angles of 13° and larger were useful because of shadowing of the spectrometer entrance by an internal Faraday cup mounted in the spectrometer scattering chamber. These measurements were made at 110 MeV. Because no detailed calibration was made for the solid angle acceptance of the focal plane detectors, these cross section data were normalized to the previous measurements with the plastic-NaI telescopes. The laboratory cross section and the vector analyzing power as a function of the laboratory scattering angle are shown in Fig. 4 where the solid

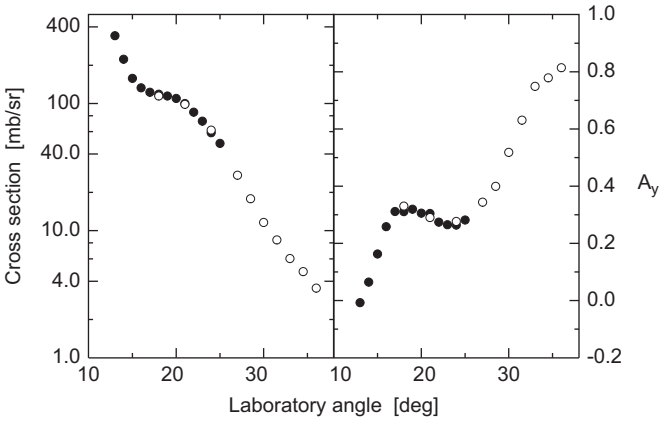

Fig. 4. Measurements of the laboratory differential cross section (left) and vector analyzing power (right) as a function of the laboratory scattering angle for 110-MeV deuteron elastic scattering from a natural carbon target. The solid symbols represent measurements made with the Big Bite Spectrometer; the open circles represent measurements made with plastic scintillator and NaI detector telescopes located at the IBP.

symbols represent normalized BBS data and the open circles IBP data. The statistical errors are smaller than the symbols and are not shown.

In order to obtain estimates of the first and second logarithmic derivatives of the cross section and analyzing power shown in Fig. 4, these two angular distributions were reproduced with a polynomial. The values of the polynomial were averaged over the range of the acceptance of the Phoswich detectors with a weight representing the circular detector acceptance. These values, calculated for a number of points close to 18°, gave estimates of the derivatives. They are $\partial\sigma/\sigma\,\partial\theta = 0.105/\mathrm{deg}$, $\partial A/A\,\partial\theta = -0.251/\mathrm{deg}$, and $\partial^2 A/2A\,\partial\theta^2 = -0.049/\mathrm{deg}^2$.

For comparison with the measurements of Figs. 2 and 3, the position displacement was converted into an angle displacement using $\Delta\theta = (\Delta x/R)\cos\Theta$ where $\Theta = 18°$ is the scattering angle and $R = 50$ cm is the distance from the target to the front face of the detector. The two straight lines in Fig. 2 have nearly the same slope, which is 0.116/deg with a difference of less than 1% between the polarized and unpolarized cases. This measurement differs from the value of the coefficient of the $\Delta\theta$ term in Eq. (8), which is 0.105/deg for the unpolarized case and 0.107/deg for the polarized case. Such a difference could easily arise from the angular distribution of the non-elastic events included in the IBP data set.

More relevant to the situation here is the reproduction of the cross ratio asymmetry. The quadratic curvature and slope for the curve shown in Fig. 3 do not result from a fitting procedure, but are given by the coefficients in Eq. (10) for the $(\Delta\theta)^2$ and $u(\Delta\theta)$ terms. The zero offset is adjusted to give a reasonable agreement with the measured asymmetries. The good representation of both the slope and curvature attest to the changes in the cross ratio asymmetry arising from second-order contributions from the beam displacement and from the difference in the vector beam polarizations for the two states used in the analysis. No attempt was made to check the systematic error arising from the zero shift induced by the term quadratic in u.

2.4. Summary of the KVI experiment

The cross ratio method for extracting an asymmetry using a left–right detector system and two oppositely polarized beam states is insensitive to first-order geometric error contributions other than the detector acceptance and luminosity changes that

cancel in the construction of Eq. (9). A Taylor series expansion of the effect on the measured cross ratio asymmetry of systematic errors in beam angle and the difference in polarization magnitudes between the two polarized beam states shows that it is also insensitive to angle (and by inference to position) shifts on target and polarization magnitude differences since Eq. (10) has no term linear in $\Delta\theta$ or u. It does, however, contain quadratic combinations of $\Delta\theta$ and u, and thus fails to cancel contributions at second order in these two errors. In the experiment conducted for deuteron-carbon scattering at the KVI, these second-order systematic errors were of the order of 1% of the cross ratio asymmetry for beam shifts on target of a few millimeters.

Using measurements made earlier at the KVI for the elastic scattering angular distributions, we were able to estimate the sizes of the coefficients in the error expansion. There is qualitatively good agreement with the results of the systematic error study, which could be expected since at 18° the particle flux into the detectors was dominated by elastic scattering. This confirms the simple analysis based on a Taylor expansion of the errors. Tests made at the other scattering angles generated cross ratio measurements where the changes in the asymmetry were not statistically significant due to the lower cross section and counting rate.

In principle, any of the measurements shown in Figs. 2 and 3 could be corrected to yield a better measurement of their particular asymmetry if this calibration of the sensitivity to systematic errors was available and the size and nature of the systematic errors were known for the time of the measurement. In the next section, a scheme is presented that uses a driving term derived from the data to determine this correction. A more extensive systematic error study was completed using the COSY storage ring to confirm this new analysis.

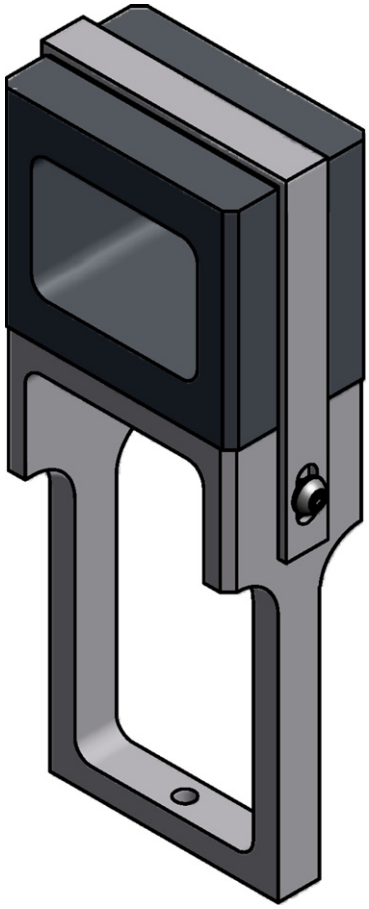

Fig. 5. Isometric view of the carbon target and its holder for use at COSY. The target was made of carbon 15 mm thick and with a rounded-corner rectangular opening that measured 20 mm by 15 mm.

3. Investigation of a systematic error correction procedure at COSY

3.1. Introduction

In the search for the existence of an EDM, a non-zero value would be signaled by a small change in the vertical component of the polarization during the course of a beam store. This change would result from the rotation of an initial longitudinal polarization about the radial axis. Since the vertical component may not vanish at the start, the polarization must be monitored as a function of time during the store. This also provides the opportunity to have information on the horizontal polarization from the measurement of a down–up asymmetry. This information can be used to correct the ring fields in order to maintain the polarization along the same direction as the velocity. To obtain sensitivities to a change in the vertical asymmetry as small as 10^{-6}, the number of recorded events needs to be large. This requires as thick a target as possible. Polarimeters mounted, for example, on the focal plane of a spectrometer have achieved efficiencies above 1% [11,12]. The efficiency is defined by the ratio of useful events scattered into the detector divided by the number of deuterons incident on the target. The solution investigated at the COSY ring involved a carbon tube through which the beam passed that was 1.5 cm thick along the beam direction, as shown in Fig. 5. This opening was rectangular (with rounded corners) with dimensions of 2.0 cm horizontal and 1.5 cm vertical. Outside this opening, the lateral thickness of the carbon material was 0.4–0.5 cm. The beam was steered close to the top edge and white noise was applied to a pair of vertical electric field plates upstream to increase the phase space of the beam along that axis. This slowly extracted the beam by bringing deuterons onto the front fact of the target. The top edge was chosen to maintain left–right symmetry. The question was whether in practice this method led to adequate efficiencies.

One of the simplest designs for an EDM polarimeter would be large acceptance detectors that would count all events above some threshold. They would be arranged to cover angular ranges where the rate and polarization sensitivity are high. Some particle selection could be provided with absorbers similar in function to those used at the KVI IBP. The EDDA detector system of crossed scintillator bars [13,14], located in one straight section of the COSY ring, matches these requirements well. A new electronic readout system was provided that was more closely suited to the response expected for an EDM polarimeter. Scintillator ring and bar signals were summed to produce functional units corresponding to left, right, down, and up scattering. Each combination was provided with a threshold that selected events to be counted in a scaler.

The run plan consisted of rapidly (on every new store) changing the beam conditions so that the position and/or angle of the beam on target was different by several millimeters or milliradians. This introduced large errors that changed the asymmetry. The goal of the study was to determine whether there was sufficient information in the detector count rates to calculate a correction for these errors.

The four count rates associated with left or right detectors, and up $(+)$ or down $(-)$ polarization, can be reconfigured to give three pieces of information other than the cross ratio. The combination based on $\sigma_L(+)\sigma_R(+)/\sigma_L(-)\sigma_R(-)$ is primarily sensitive to the relative luminosity for the two polarization states and is not useful here. This leaves two remaining combinations. One is

given by

$$\phi = \frac{s-1}{s+1} \quad \text{where} \quad s^2 = \frac{\sigma_L(+)\sigma_L(-)}{\sigma_R(+)\sigma_R(-)} \tag{15}$$

which is sensitive to a left–right geometric error in first order while suppressing the sensitivity to the beam polarization. This driving term will be investigated as a possible input from which to calculate corrections for geometric errors. Since this is the only such combination that remains based on the original data, it must suffice for both position and angle misalignments. Indeed, the error parameterizations given earlier as a function of angle (θ) could equally well have been considered as a function of position (x). These two variables are related at forward scattering angles through R, where $x=R\theta$ and R represents an effective distance to the detector.

The last piece of information that may be taken from the four count rates is the total rate itself, which can be represented as the sum of the count rates per unit time. Choosing this as the second driving term (W) provides a handle for systematic errors that are a function of the counting rate. Such errors arise, for example, from changes in detector gain or threshold as rates change or from events that are pushed above threshold by virtue of being added to other events in the electronic signal (pileup). This raises the question of whether rate and geometry issues can be treated separately and, if so, how.

3.2. Details of the COSY experiment

The polarized deuteron beam was generated in an atomic beam source [15] with two stages of sextupole separator magnets, each followed by RF transition units. This provided many possible combinations of vector (p_V) and tensor (p_T) polarization. Those chosen for this experiment are summarized in Table 1 where the first two columns give the nominal vector and tensor polarization under ideal conditions. In addition to two states that emphasized vector polarization only and two that contained tensor polarization, there was a nominally unpolarized state. The D^- beam was accelerated through the injector cyclotron and sent into the transfer line at 76 MeV where a Low Energy Polarimeter (LEP) is located utilizing a thin carbon rod target with its long axis vertical. Deuteron elastic scattering was observed with four NaI detectors mounted at the same laboratory angle of 40° in the left, right, down, and up directions. The left–right asymmetry was used to measure the vector polarization of each state based on an analyzing power of $A_y=0.61\pm0.04$ [14] (or $iT_{11}=0.52\pm0.03$). The polarizations obtained there are shown in column 3 of Table 1. In each case, the number in parentheses is the statistical error. At the LEP scattering angle, there is very little sensitivity to the tensor polarization of the beam; data comparing down and up detector rates with left and right detector rates was not used in the analysis. Data from the LEP could be produced only when the pulses for the COSY storage ring were passing through the injection beam line and hitting the rod target. In order to improve the statistical precision of these data, additional injection pulses were generated during the ring storage time; these pulses were not sent into the ring.

The running time devoted to this experiment was divided into several "periods" with different running conditions based on average beam intensity, polarized ion source setup (ionizer solenoid normal or reversed), and polarization state performance. For the results illustrated in this section, data from the longest and most stable of these periods was chosen. The results from other periods were similar. Polarization values from the EDDA detector data will be discussed later.

The D^- beam from the transfer line was strip-injected into the COSY ring. During the acceleration of polarized deuterons to the momentum of the experiment, no spin resonances were crossed [16]. No electron cooling was used. The beam was bunched and ramped to a momentum of $p=0.97$ GeV/c ($T=235$ MeV), after which the bunching was turned off and the beam allowed to coast. During this operation, the carbon tube target was in place and the beam was always kept inside the opening of the tube. For this experiment, the upper horizontal edge of the tube opening was used as the extraction point. This edge was placed at the nominal center of the COSY beam pipe to a precision of about 0.1 cm, which also centers it on the EDDA detector scintillators. During injection and acceleration, steering magnets were used to keep the beam in the center of the tube opening. Just before extraction and data taking began, the beam was raised until its center was 0.3 cm below the edge. The number of deuterons per fill varied in the range from 3×10^8 to 1×10^9 as measured by the beam current transformer (BCT).

Extraction of the beam was accomplished by increasing the size of the beam's vertical phase space. For a controlled vertical beam blow up, a stripline kicker unit switched to the vertical excitation mode was used with band-limited white noise covering only the vertical betatron oscillation frequencies. The power of the white noise was chosen so that within the 55 s of the data acquisition period about 90% of the beam was lost. It was assumed that these losses were on the tube target, making it the limiting aperture in the storage ring. Fig. 6 shows a typical dependence of the circulating current as measured by the BCT.

Table 1
Deuteron polarization data from the Low-Energy Polarimeter (LEP) and EDDA.

State	Nominal p_V	Nominal p_T	LEP p_V	EDDA p_V	EDDA p_T
V−	−2/3	0	−0.520(2)	−0.5370(6)	−0.128(3)
V+	+2/3	0	0.396(2)	0.4013(6)	0.068(3)
T−	1/2	−1/2	0.349(2)	0.3399(7)	−0.361(4)
T+	−1	1	−0.702(2)	−0.7311(7)	0.620(4)

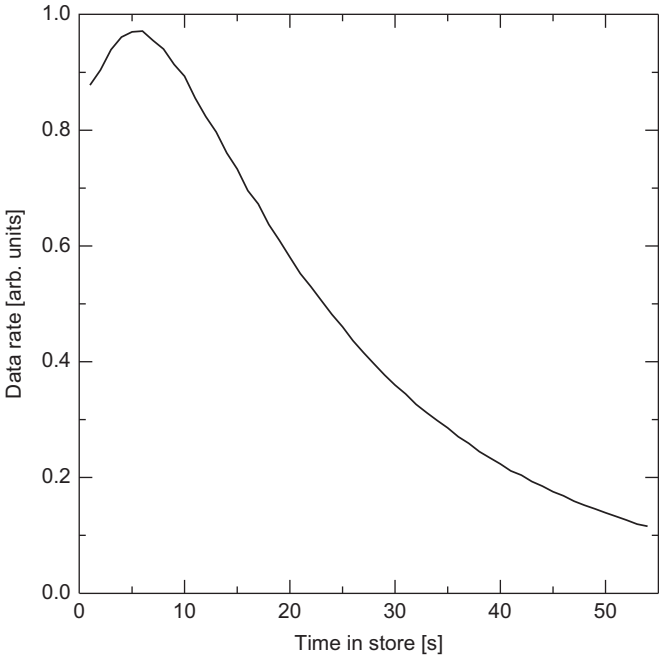

Fig. 6. Measurements of the count rate in the detectors as a function of time in the store. The rate axis is in arbitrary units.

The COSY control system allowed for the use of a series of beam setups with a different one being applied to succeeding stores. As the purpose was to determine the sensitivity to large position and angle beam misalignments at the target in the horizontal plane, the steering magnets were arranged to provide displacements from the center position of $\Delta x = -2, -1, 0, 1$, and 2 mm and angle displacements of $\Delta\theta_x = -5.0, -2.5, 0, 2.5$, and 5.0 mrad. Since the detectors were located about 1 m away from the target, the angle changes were expected to generate larger systematic errors than the position changes. The range of changes in both cases was limited by the transverse acceptance of the COSY ring.

The signals obtained from the EDDA detector came from the outer layer of scintillator bars and rings. There were 32 bars that ran parallel to the beam. These were ganged together into 4 groups of 8 detectors, each group centered on the left, right, down, and up directions. Each of the scintillator bars was cut with a triangular cross section since, in the original EDDA experiment, azimuthal angles were determined by the energy sharing of a signal between neighboring bars. For the polar scattering angle, EDDA has a series of ring detectors, each of which wraps around half of the bar detectors. Two such detectors together cover an entire circle at a constant scattering angle. The forward three ring sets (excluding a small triangular scintillator) were ganged together to make the "front" detector and the next three the "back" detector. This produced data for two polarimeter systems that operated in parallel. The extreme scattering angle ranges for these two sets were 9.0° through 13.2° and 11.7° through 16.9°. As was the case for the bar detectors, the ring detectors as seen from the target overlap their neighbors in such a way as to provide scattering angle information through energy sharing along each track. Such sharing was not used in the analysis.

The goal of the discriminator and logic circuit was to provide a trigger to each combination, or "patch," consisting of one bar group and one ring group. The PMT anode signals for each patch were summed and the result sent to a lower level discriminator. All of the eight discriminator outputs were sent into a logical array. In this application, the successful output for a patch required a threshold crossing for the four patches that shared the same ring set and the two patches that shared the same bar set, for a total of five patch inputs. The common ring and bar in this combination was the location of the desired patch. Signals on the other three patches were required to be absent. This scheme provided a total of eight outputs that were routed to scalers. The scaler units were gated on after the beam was positioned and extraction begun, then gated off 55 s later as the store was dumped in preparation for the next beam injection. Additional inputs were used to encode the polarization state and the particular value of the systematic error being generated by the machine controls. The scalers were recorded in the computer every 0.1 s. Prior to the run, voltage settings on all of the photomultiplier tubes were adjusted to provide the same gains for inputs in the same detector sets. A common threshold was used for all logic module inputs. During this setup period, analog signals were also fed to ADCs so that a pulse height spectrum could be generated. This was not done during normal data acquisition in order to minimize the dead time for processing each event. Pulse height spectra were taken periodically to confirm that all detectors were working properly.

The information from the data acquisition system at the end of each scaler readout chain consisted of asymmetries as in Eq. (8) for the left–right detector pair and the down–up detector pair for each polarization state. In addition either the two vector polarized states or the two tensor polarized states were combined to form a cross ratio as in Eq. (9), again for both the left–right and down–up detector pairs. Lastly, the four count rates were combined to yield an asymmetry sensitive to tensor polarization:

$$\varepsilon_T = \frac{\sigma_D + \sigma_U - \sigma_L - \sigma_R}{\sigma_D + \sigma_U + \sigma_L + \sigma_R} = \frac{\sqrt{6} p_T T_{22}}{\sqrt{8} - p_T T_{20}} \tag{16}$$

where p_T is the Cartesian tensor polarization from the polarized ion source. All of this information was available separately for events recorded in the front and back sets of EDDA detector rings.

3.3. Polarimeter efficiency

All events that were above threshold were counted in the scaler array and considered good polarimeter events. The efficiency of the polarimeter is defined as the number of events recorded in a given period of time divided by the number of deuterons lost from the stored beam during that same time period. This efficiency should be at least an order of magnitude below the EDM design goal of about 1% because polarimeter events were not observed for angles between 5° and 9° and because the thickness of the tube target was limited by the beam line geometry to 1.5 cm. The stored beam current was monitored using the BCT.

It was expected that the maximum efficiency would be obtained when the direction of the beam was parallel to the inside surface of the tube where the beam was being extracted. Fig. 7 shows a set of efficiency measurements for the front and back detector systems as a function of the angle of vertical beam tilt. The efficiency goes through a maximum between 0.5 and 0.7×10^{-3} at about 3 mrad. The angle offset appears to be an artifact of the calibration of the beam angle associated with particular steerer settings.

The shape of the efficiency curve was simulated using a Monte Carlo program to calculate the contributions of multiple angle straggling [17] to the number of deuterons that exited the inside face of the target without going through its full thickness. Such losses decrease the efficiency of the polarimeter and become more severe when the beam is not aligned with the target surface inside the tube. In order to model the shape of the efficiency curve, it is necessary to assume that the target front face is illuminated according to some distribution. In this case, an exponential function was used with a $1/e$ width of 0.2 mm as the deuteron impact point moved up the target front face. That choice resulted in the calculation shown in Fig. 8. The solid line is the result of the Monte Carlo calculation and the dashed lines indicate the statistical error band. The solid points are the

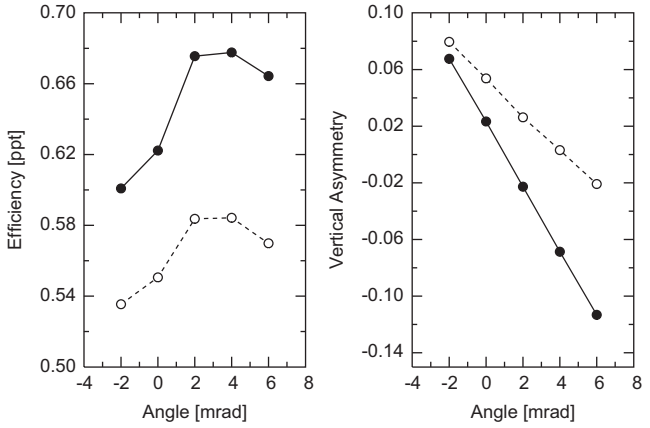

Fig. 7. (Left) Measurements of the polarimeter efficiency for the front (solid) and back (open) EDDA ring detector sets as a function of the angle of vertical tilt at the tube target. (Right) Measurements of the down–up asymmetry (like Eq. (8)) for the unpolarized state as a function of the angle of vertical tilt. The symbol sets are the same as for the left panel.

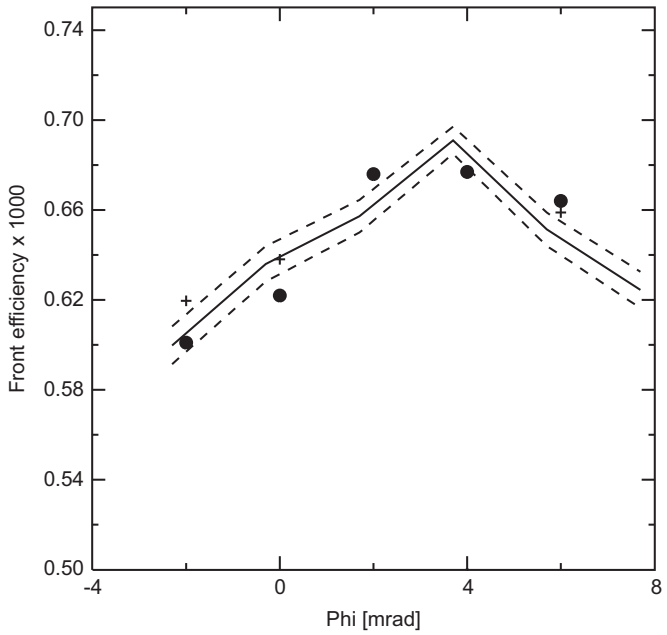

Fig. 8. Measurements of the efficiency (solid dots) of the front detector system as a function of the vertical angle of the beam. The efficiency for the back detectors has been scaled upward to match the front efficiencies at 2 and 4 mrad. The solid curve is the prediction of a Monte Carlo simulation including multiple angle straggling. The dashed lines represent the size of the Monte Carlo statistical error. It has been offset to match the efficiencies plotted here and shifted by 3.8 mrad to the right to align with the maximum efficiency.

efficiencies of the front detector system as a function of the vertical tilt angle. The back detector efficiencies exhibit a similar shape with angle. They have been rescaled upward to agree with the front efficiencies for the 2 and 4 mrad points. At other angles, they are represented by the plus symbols. Since the importance of this comparison is in the shape with angle, the scale of the Monte Carlo result was also scaled to best agree with the front detector efficiencies. This yields 6.9×10^{-4} as the front system efficiency and confirms the choice of 0.2 mm as the average flux spread above the target edge.

To establish whether this result meets expectations for the polarimeter, it must be compared with a computer simulation of deuteron transport through the target and a nuclear scattering or reaction leading to a polarimeter event. The energy loss of protons and deuterons in various materials was obtained from the tables of Janni [18]. Deuteron losses were scaled from those for protons. Straggling in the energy loss and small changes to the particle direction were calculated using the distribution width as given by Marmier and Sheldon [17]. Cross section and vector analyzing power angular distributions for deuteron elastic scattering from carbon were determined from an interpolation formula that connected the measurements of Okamura [19], Bäumer [20], Kawabata [21], and Satou [22]. Angular distributions for deuteron inelastic scattering, (d,p) reactions, and deuteron breakup were obtained by scaling the measurements at lower energy made with the NaI detector system at the KVI. There may be substantial errors in this extrapolation. Particles scattered from the target were tracked through the beam pipe, crossed fiber scintillators, and plastic scintillators of the EDDA detector system. Simulations of the energy deposited were used to determine the settings of the signal threshold for the simulation. The predictions for the efficiencies were 5.7 (front) and 4.7 (back) $\times10^{-4}$, somewhat below the measurements. These differences are within the uncertainties of the model, which are dominated by the errors in scaling the reaction cross sections and analyzing powers.

It is important to note that the efficiency associated with either the horizontal or vertical asymmetry measurements is only half of these values.

The level of agreement reported here between the efficiency measurements and the Monte Carlo predictions validates the use of a thick carbon target mounted close to the beam for such polarization measurements. When a thicker target and smaller scattering angle limits are included in the calculation, efficiencies of approximately 1% are obtained.

3.4. Model of the systematic error effects

It is possible to examine subsets of the measurements, such as the KVI cross ratio data discussed in the previous section, and make comparisons with formulas for second-order errors. But with a much larger set of error effects and many things that could influence them, it seemed appropriate to formulate a more comprehensive model of such effects. The goal is to explain all of the aspects of the set of data from COSY and, by requiring that the model reproduce those data, extract values for the various strengths (logarithmic derivatives, for example) that connect the deliberately-created systematic errors with measured changes in the asymmetries. Doing so would hopefully reveal what systematic effects were important during this study and yield information about their size in a situation that was expected to be similar to that for an EDM polarimeter.

At the beginning of the experiment, the run plan was focused on errors having to do with geometry changes. However, once the run was underway, it became clear that the data were also being influenced by the instantaneous data acquisition rate. The cause of this dependence was traced to the appearance of 50 Hz ripple on the data rate as if the vertical position of the beam on the target was oscillating with the power line frequency. The result was that most events came within a small time window that was of the order of 1% of the available time, thus increasing the instantaneous data acquisition rate by about two orders of magnitude. Rather than trace and repair this problem, it was decided to use it as an opportunity to study rate as well as geometry effects. Beam currents were reduced in an effort to reduce the size of the rate effects, and to an extent this proved helpful. Fig. 9 shows a set of cross ratio measurements averaged over position and angle error and plotted as a function of time during the store. The shape of these data shows a downward hook at the beginning followed by a slow rise until the end. This shape is identical to the count rate illustrated in Fig. 6. This shape is offset along both axes so as to fit the cross ratio measurements. To make this comparison more quantitative, Fig. 10 shows the cross ratio as a function of the instantaneous data acquisition or count rate. The dependence is linear. Such an effect was universally observed throughout the set of data acquired on this experiment.

With a linear dependence of polarization observables on the instantaneous rate, the separation of geometry and rate effects became easy. The data from each type of store (asymmetry observable, polarization state, and geometric error) was fit to a straight line as a function of the instantaneous rate for the detectors contributing to that observable. The zero-rate intercept was taken as the raw data for the analysis of geometric corrections. The slope was taken as the measurement of the rate effect. In this way, these two parts of the experiment were decoupled. We will discuss these effects in separate subsections below.

3.4.1. Modeling geometric systematic errors

The model of geometric effects was expected to be the most complicated. Rather than derive the influence on the measurements of each effect using a Taylor Series expansion as in Eq. (10), these

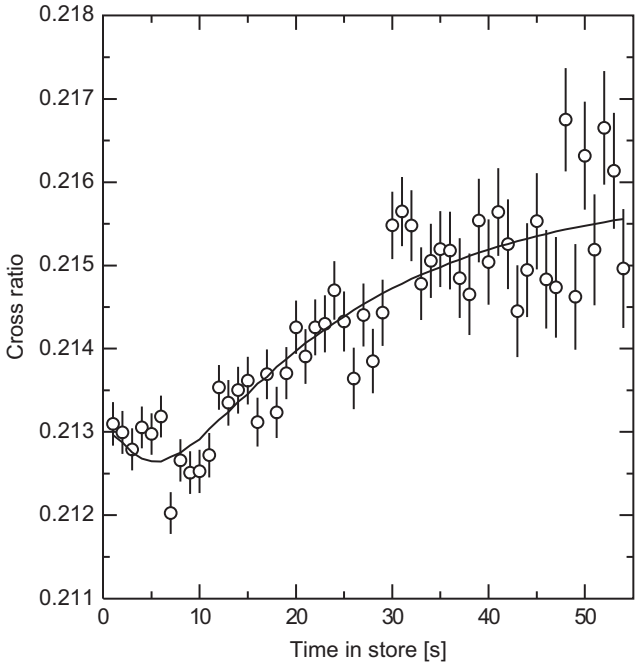

Fig. 9. Measurements of the cross ratio asymmetry for the front detector system averaged over position and angle error and plotted as a function of the elapsed time during a store. The curve is taken from Fig. 6 and adjusted in offset and scale to match these data, thus confirming the correlation between cross ratio changes and the instantaneous data taking rate.

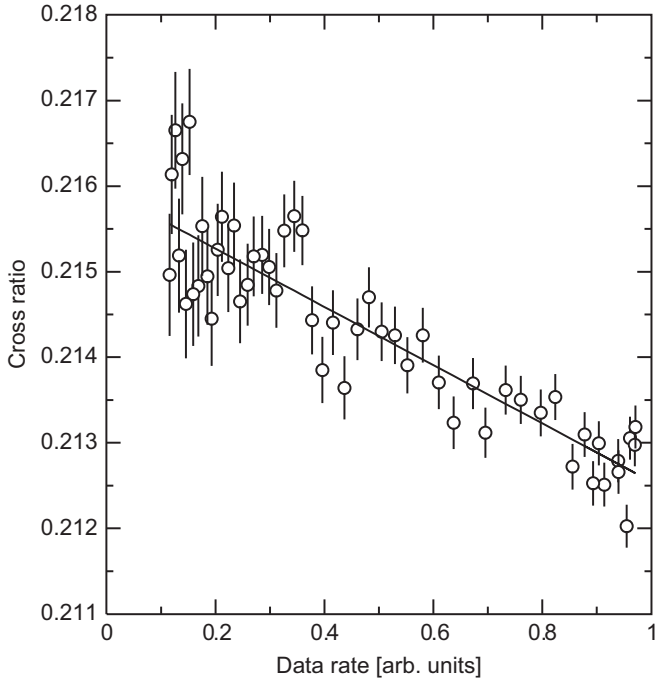

Fig. 10. Measurements of Fig. 9 as a function of the instantaneous count rate in arbitrary units. The line is a least squares straight line fit to these measurements.

effects were incorporated into a computer calculation of the asymmetries by modifying the polarized cross section formula of Eq. (1). This would ensure that no connections or correlations among effects would be overlooked. Finally, the amplitude or magnitude of each effect was determined by fitting all the data and adjusting the size of each amplitude using a non-linear regression algorithm [23]. The following effects were expected to be present in the model:

Beam polarizations: While there was information on the size of the vector polarization in each polarization state from data collected with the LEP, the data from EDDA had a much greater statistical precision. Thus the vector and tensor polarizations for each of the polarization states were introduced as adjustable parameters for a total of eight variables. These polarizations are listed in the two right-hand columns of Table 1.

Analyzing powers: The sensitivity of the detector system to vector and tensor polarization was included through an analyzing power for each detector element with different values for the front and back ring detector systems. For the tensor asymmetry defined in Eq. (16), the parameterization was $\varepsilon = 2p_T A_T$, ignoring the influence of the T_{20} term. For either front or back detectors, this added two variables.

Solid angle ratios: The actual asymmetry might differ because of unequal acceptances among the bar segments of the detector. So three solid angle ratios were introduced: left/right, down/up, and (down+up)/(left+right), for three more variables.

Logarithmic derivatives of position or angle: If there are shifts of position or angle, these should appear as changes to the average cross section or analyzing power for a detector patch. As discussed in the previous section, these may be described using logarithmic derivatives of the cross section or analyzing power with respect to either position or angle. It was decided that, in anticipation of being able to correct for both position and angle misalignments using one correction parameter, it would be appropriate to include derivatives of only one position or angle. The relationship between the two would be managed through the introduction of the effective distance to the detector introduced earlier. To carry this to second order for both vector and tensor analyzing powers requires the introduction of seven variables, including the effective distance. Again, there is a separate set of these for the front and back detector systems.

These 20 variables proved inadequate to account for all of the effects seen in the measurements. It thus became essential to add additional features to the model of geometric effects. These included the following:

Polarimeter rotation angle: A small component of the vector beam polarization appeared in the vertical asymmetries like Eq. (8). This was due to a breaking of the symmetry between left and right in the construction of the EDDA ring detectors. The rings were divided into two pieces. Each went around the left or right half circle but was then brought to the middle on either the top or the bottom where it was connected to the photomultiplier tube. An angle of rotation was introduced that determined the mixing of the vertical component of the polarization into the measurement of the vertical asymmetry.

Beam position and angle mixing: The effects of changes to horizontal position and angle also appeared in the vertical asymmetry measurements. These could be introduced if a horizontal change, through a coupling in the beam optics, also created a change in the vertical beam position or angle. Two such coupling parameters were introduced, one for position and another for angle.

Low momentum tail: Some number of particles that encounter the inner surface of the tube target undergo only a small energy loss. This results in a slight lowering of their momentum. If such particles are not lost somewhere in the ring, they may return to the region of the EDDA polarimeter where they can strike the right detector, which lies on the low momentum side of the ring plane. Such a process significantly increased (up to 30%) the rate in the right-side detector patch for both front and back systems. Assuming that this rate was independent of polarization still permitted an adequate representation of the measurements.

However, it was important to introduce a dependence of this rate on position and angle changes separately.

Together, these additions led to 26 polarization and geometry variables for the model. The 8 polarizations are listed in Table 1 above and the remaining 18 parameters, including the analyzing powers, are listed in Table 2 below. The model is summarized by listing the way in which the four count rates, L, R, D, and U, were calculated for the four patches on the polarimeter, as shown in Eq. (17) for an angle misalignment. Parameters from the model are noted by C_i, which are associated with particular entries in Table 2:

$$\sigma_L = \sqrt{\frac{C_2}{C_{15}}}[1-C_3\Delta\theta+C_4(\Delta\theta)^2][1+p_V C_5(1-C_6\Delta\theta+C_7(\Delta\theta)^2) -p_T C_8(1-C_9\Delta\theta+C_{10}(\Delta\theta)^2)] \quad (17)$$

$$\sigma_R = \sqrt{\frac{1}{C_2 C_{15}}}[1+C_3\Delta\theta+C_4(\Delta\theta)^2][1-p_V C_5(1+C_6\Delta\theta+C_7(\Delta\theta)^2) -p_T C_8(1+C_9\Delta\theta+C_{10}(\Delta\theta)^2)]+C_{16}[1+C_{18}\Delta\theta]$$

Table 2
The geometry error parameters described under "Name" appear as the C_i in Eq. (18) and took on the values listed in the model.

C parameter	Name	Value
1	Effective detector distance	0.524(6) m
2	Left/right solid angle ratio	1 (fixed)
3	$\partial\sigma/\sigma\partial\theta$	0.02561(7) mrad^{-1}
4	$\partial^2\sigma/2\sigma\partial\theta^2$	0.00029(2) mrad^{-2}
5	$iT_{11}=C_5/\sqrt{3}$	0.3884(4)
6	$\partial A/A\partial\theta$	$-0.0055(2)$ mrad^{-1}
7	$\partial^2 A/2A\partial\theta^2$	0.00008(6) mrad^{-2}
8	A_T	0.0444(2)
9	$\partial A_T/A_T\partial\theta$	0.008(5) mrad^{-1}
10	$\partial^2 A_T/2A_T\partial\theta^2$	0.0013(9) mrad^{-2}
11	Down/up solid angle ratio	1.0438(3)
12	Position mixing	$-0.032(5)$
13	Angle mixing	0.036(2)
14	Effective rotation	0.0260(5)
15	(Down–up)/(left–right) solid angle ratio	1.3046(2)
16	Tail fraction, T	0.2985(2)
17	$\partial T/\partial x$	0.0122(7) mm^{-1}
18	$\partial T/\partial\theta$	0.0086(3) mrad^{-1}

$$\sigma_D = \sqrt{C_{11}C_{15}}[1-C_3C_{13}\Delta\theta+C_4C_{13}^2(\Delta\theta)^2] \times[1-p_V C_5 C_{14}(1-C_6C_{13}\Delta\theta+C_7C_{13}^2(\Delta\theta)^2) +p_T C_8(1-C_9C_{13}\Delta\theta+C_{10}C_{13}^2(\Delta\theta)^2)]$$

$$\sigma_U = \sqrt{\frac{C_{15}}{C_{11}}}[1+C_3C_{13}\Delta\theta+C_4C_{13}^2(\Delta\theta)^2] \times[1+p_V C_5 C_{14}(1+C_6C_{13}\Delta\theta+C_7C_{13}^2(\Delta\theta)^2) +p_T C_8(1+C_9C_{13}\Delta\theta+C_{10}C_{13}^2(\Delta\theta)^2)]$$

If these equations are used for a position misalignment, the numerical value in millimeters is divided by C_1 and used in place of $\Delta\theta$, which is in milliradians. At the same time C_{12} replaces C_{13} and C_{17} replaces C_{18}. From these rates the asymmetries are calculated as shown in Eqs. (8), (9), and (16).

Attempts to determine these variables revealed that there was a significant correlation among a few variables that gave comparable values of χ^2 over a wide range of variable choices. Since this correlation pattern involved the beam polarizations, which were known with lower statistical precision from the Low Energy Polarimeter, it was possible to determine approximately where the correct answer was located. In order to constrain the fitting procedure to a normal process of convergence, it was decided to fix the left–right solid angle ratio for the front system to one, a choice that also gave good agreement between the EDDA and Low Energy Polarimeter vector beam polarizations. Once determined, these polarizations were also fixed for the back detector system and other parameters were allowed to vary, including the left–right solid angle ratio.

Figs. 11–15 show a series of polarization and correction observables for the front set of EDDA ring detectors. For each case, the panels show different polarization states or combinations of polarization states as appropriate. Within each panel, the observable is plotted as a function of the nominal error in either millimeters (upward pointing triangles) or milliradians (downward pointing triangles). For the part of the experiment chosen for illustration, the solenoid in the ionizer region of the polarized ion source was set with its polarity reversed. Thus the "V+" state has a negative vector polarization and will yield a negative asymmetry. The values in Table 1 have the normal polarity. In all cases, the lines on the graphs are calculated from the model. For each of the figures, the comments in the discussion to follow will point out the main sensitivities to derivatives and other features of the

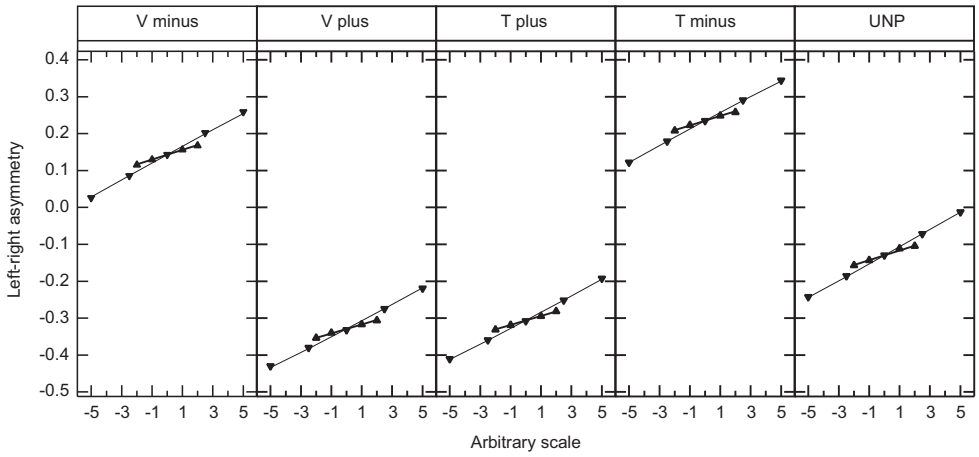

Fig. 11. Measurements of the horizontal asymmetry (Eq. (8)) for each of the five polarization states as a function of either the angular error (mrad, down-pointing triangles) or the position error (mm, up-pointing triangles). Model calculations are shown by thin (thick) lines for the angle (position) errors. These data represent a selected part of the entire experiment (see text) and the data using the front ring detectors.

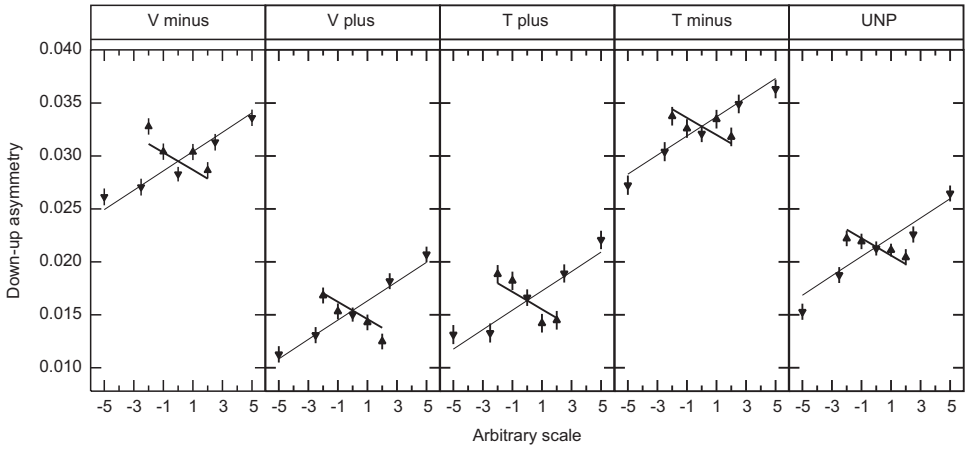

Fig. 12. Like Fig. 11, except that the measurements are for the vertical asymmetry (Eq. (8)).

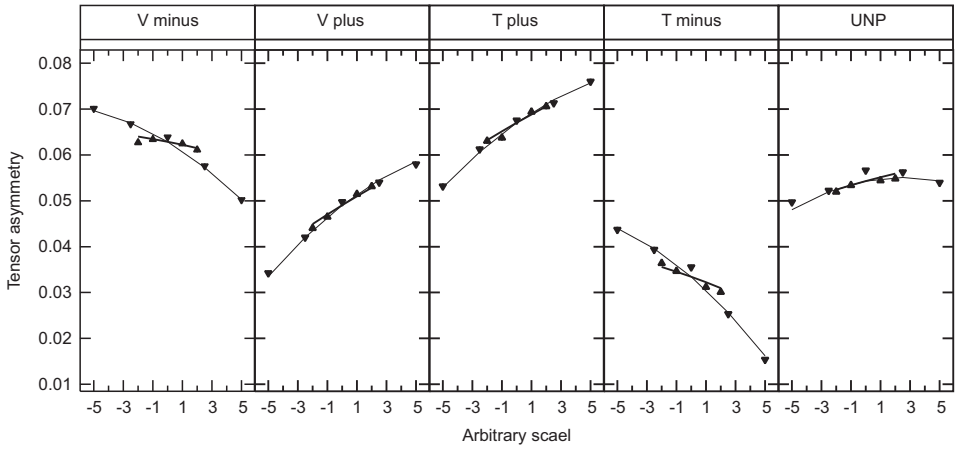

Fig. 13. Like Fig. 11, except that the measurements are for the tensor asymmetry.

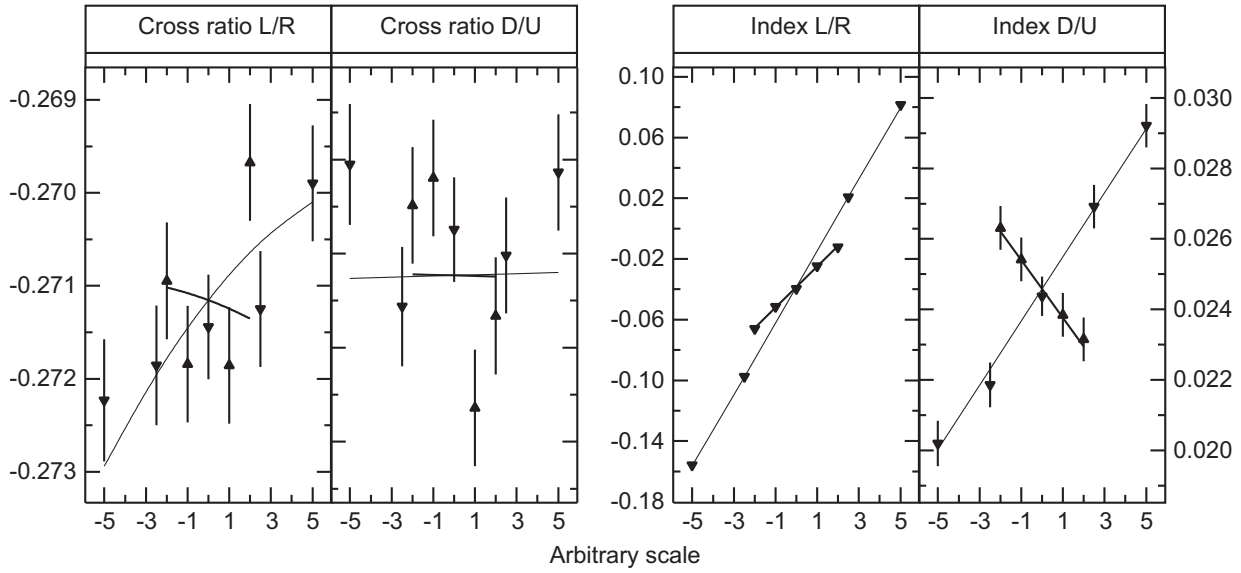

Fig. 14. Like Fig. 11, except that the left panels show the cross ratio and the right panels the geometric driving term. In each pair the left panel is for the horizontal direction and the right panel is for the vertical direction. These data are taken from the two tensor polarized states.

polarimeter parameter list. While the main sensitivity may lie there, in fact all parameters were adjusted to reproduce all data, so other measurements contribute to the final values and errors in the model parameters.

The asymmetries in Fig. 11 are obtained from the left–right comparison of Eq. (8). The "up–down–down–up" pattern of the first four panels follows the sign and magnitude of the vector polarization for each of the states in the title. The last panel is for

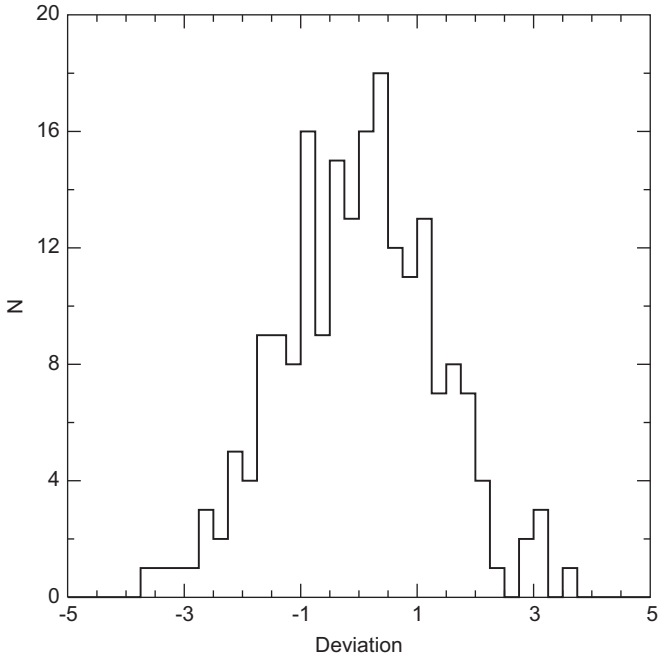

Fig. 15. A histogram where each entry represents the ratio of the fit residual from the model divided by the statistical error for the entire set of observables calculated for the data shown in Figs. 11–14. The reduced χ^2 for this fit is 1.7.

the unpolarized beam; it is negative because of the excess count rate in the right counter due to the low-momentum tail. With the left–right solid angle ratio fixed to equal one, the tail fraction becomes $C_{16}=0.2985(2)$ where the value in parentheses is the statistical error from the least-squares fitting procedure. The tail fraction was modified by two coefficients that multiplied the Δx and $\Delta\theta$ error terms. Those coefficients are $C_{17}=0.0122(7)\,\mathrm{mm}^{-1}$ for Δx and $C_{18}=0.0086(3)\,\mathrm{mrad}^{-1}$ for $\Delta\theta$. The unpolarized asymmetry measurement sets the reference against which the other asymmetries measure the polarization. The values (without the solenoid sign reversal) for the vector polarization are given in Table 1. With these polarizations, the analyzing power becomes $iT_{11}=C_5/\sqrt{3}=0.3884(3)$.

The left–right asymmetry should be sensitive to systematic geometry errors in first order, and this is demonstrated by the large linear effects seen in all five polarization states. The size of this slope is given by $\partial\sigma/\sigma\partial\theta-(\partial A/A\partial\theta+\partial\sigma/\sigma\partial\theta)\varepsilon^2$ in the case of the angle-dependent measurements (see Eq. (8)) where ε is the vector asymmetry. The varying size of the asymmetry ε from one spin state to another makes it possible to determine both derivatives, and the results are $C_3=\partial\sigma/\sigma\,\partial\theta=0.02561(7)\,\mathrm{mrad}^{-1}$ and $C_6=\partial A/A\partial\theta=-0.0055(2)\,\mathrm{mrad}^{-1}$. The slope for the position motion in Fig. 11 is less, and the effective distance to the detector is given by $C_1=x/\theta=52.4(6)$ cm. This is slightly larger than half the actual distance to the detector, and may reflect acceptance limits set by the edge of a crossed fiber array from the EDDA detector that is located at this distance. The effective distance is 120(4) cm for the rear detector, a value more in accord with the real distance.

The value of the logarithmic derivative of the cross section should also be consistent with the effects on the down–up asymmetry in the case that a vertical angle change is made in the beam. The right-hand panel of Fig. 7 shows such results for the case where tests of the effect of the vertical angle on the polarimeter efficiency were conducted. For the front detector (solid symbols), the slope of this dependence is $-0.023\,\mathrm{mrad}^{-1}$, a value that agrees well (in magnitude) with the value for the logarithmic derivative of the cross section for a horizontal angle change. The calibration of such angle changes depends on the precision of the lattice calculation of the beam optics; thus such a calibration change may be the most important contributor to the difference in these slopes.

Fig. 12 shows the same information for the down–up asymmetry. The displacement of the unpolarized state measurements from zero gives a value for the down–up solid angle ratio of $C_{11}=1.0438(3)$, indicating that the down detector has the higher count rate. There is again the "up–down–down–up" pattern associated with the vector polarization values, so there is some sensitivity to the vertical component of the polarization. This comes about because the ring detectors are connected to photomultiplier tubes that are mounted along a vertical axis but connected to scintillators that bend either to the right or left as they wrap around the bar scintillators. Through attenuation in the ring scintillators, events from one side are emphasized in a system where all events share a common threshold. The rotation parameter that describes this effect is $C_{14}=0.0260(5)$. The other feature of the vertical asymmetry is that horizontal position and angle displacements matter. One explanation would be X–Y position and angle coupling in the steering of the COSY beam. The position mixing parameter is $C_{12}=-0.032(5)$ and the angle mixing parameter is $C_{13}=0.036(2)$.

Fig. 13 shows the same information for the tensor asymmetry. The offset of the unpolarized asymmetry from zero is parameterized by the (down+up)/(left+right) solid angle ratio whose value is $C_{15}=1.3046(2)$. This number is large to counteract the effects of the tail fraction, which is about the same as the fractional part of this value. The "up–down–up–down" pattern here represents the changing tensor polarization associated with each polarization state. The tensor polarization in the nominally vector polarized states is smaller than that for the tensor polarized states, but it does not vanish. For the tensor polarization, there is no guidance from the Low Energy Polarimeter. Thus the tensor polarizations (p_T) for the T+ and T− states were initially assumed to have the same magnitude as the vector polarization for these states but with opposite sign. Then the tensor asymmetries for each of the polarization groups were used to calculate a "tensor analyzing power" such that it obeys $\varepsilon_{TENS}=p_T A_T$. All of the values for A_T across the entire experiment were averaged to give $C_8=0.0444(2)$. Then for our example polarization group, the tensor polarizations were recalculated from the observed asymmetries and can be found in Table 1.

Like the simple vector asymmetries, the tensor asymmetries show a slope that in this case varied with polarization. The pattern $(-)(+)(+)(-)$ tracks the vector polarization, and an expansion of this systematic error shows that it varies according to $-\varepsilon_V(\partial\sigma/\sigma\partial\theta+\partial A/A\partial\theta)$. These data also contribute to the values for these logarithmic derivatives and the vector polarizations. Each of these sets of points also demonstrates noticeable curvature. This comes from the second derivative $-\partial^2\sigma/2\sigma\partial\theta^2$ whose value was determined to be $C_4=0.00029(2)\,\mathrm{mrad}^{-2}$.

Fig. 14 contains panels illustrating the cross ratio sensitivity to systematic errors and the geometric driving term. For this illustration, the cross ratio for the tensor polarized states was chosen since these states provide the largest vector polarization. The two cross ratio panels are for the horizontal and vertical cases. For this asymmetry, the sensitivity to first order terms disappears. The slope of the cross ratio is given by the third term in Eq. (10) where it is shown to depend on the logarithmic derivative of the analyzing power multiplied by the difference in vector polarization magnitudes for the two polarization states that contribute to the calculation. There is a weak curvature here as well, unlike the test measurements at the KVI where this term was much larger. This curvature determines the value of the second derivative $\partial^2 A/2A\partial\theta^2$ to be $C_7=8(6)\times10^{-5}\,\mathrm{mrad}^{-2}$.

For completeness, derivatives of the tensor analyzing power were also included in the model. $\partial A_T/A_T\partial\theta$ was found

to be $C_9 = -0.008(5)\,\mathrm{mrad}^{-1}$ and $\partial^2 A_T/2A_T\partial\theta^2$ to be $C_{10} = 0.0013(9)\,\mathrm{mrad}^{-2}$. With this, all adjustable parameters for the front detector system have been determined and are summarized in Table 2. Values for the back detector system are similar.

The two right-hand panels in Fig. 14 show the geometric driving term for this polarization group. This parameter was calculated using the data from the tensor polarized states. Clear straight lines are evident, indicating that this combination is a robust measure of the deviation of the beam from its central values. No new model information is gleaned from this combination.

The quality of the model reproduction of the systematic error effects can be judged from a χ^2 distribution as shown in Fig. 15. The samples in this histogram represent the ratio of the residual for the fits shown in the model figures to the statistical error of the particular polarization observable data point. Such a distribution should ideally have a width parameter of one. In this case the reduced χ^2 for the fit is 1.7, indicating some non-statistical variations. These most likely arise from occasional stores in which something happened to the beam. Such stores were not removed from the data set. The conclusion is that this level of variation is acceptable and does not imply that there are remaining dependencies that need to be included in the model.

3.4.2. Modeling rate systematic errors

In a manner similar to that for the geometric errors, a model was produced to describe the slope with increasing rate associated with each data point in Figs. 11–14. The rate, which was available as a sum of detected events per unit time, was adjusted to a common scale for the purpose of setting values for this slope; thus the results are numerically meaningful only for relative comparisons. Fig. 16 illustrates the results associated with the simple left–right asymmetry, again taken for the selected polarization group and the front detector system. These data show a weak polarization dependence and almost no sensitivity to changes of position or angle. Thus a single value for the slope was sufficient for all cases of a given polarization observable. For the data in Fig. 16, an average value of the slope of 0.0163(6) is appropriate, and the down–up–up–down pattern for the polarized states needs a correction coefficient of $-0.011(3)$ to be multiplied by the appropriate vector polarization. Similar results were obtained for the down–up asymmetry and the tensor asymmetry. The cross ratios showed no dependence on polarization state or geometric error, thus they are represented by a single average value. All of these results are included in Table 3. The overall quality of the fit is similar to that shown in Fig. 15 for the geometry model.

3.5. Summary of experimental and model results

At the beginning of the COSY-Jülich experiment, the goal was to find a procedure that would permit correction of the second-order (and higher) contributions to the effects of systematic errors from geometrical misalignments (position and angle). Once the run was underway, the opportunity was taken to include an investigation of the effects of changing data acquisition rates. Using only information available from the polarimeter data itself, it is possible to construct two driving terms, one that depends mainly on geometrical changes and one that is a measure of the instantaneous counting rate. If these two alone are sufficient to determine how large a systematic error is present, then it may become possible to correct asymmetry measurements such as the cross ratio in real time as the data become available.

The first question is whether the geometrical driving term can be used for both position and angle changes. Fig. 17 shows a set of measurements of the left–right asymmetry for the T− polarization state (fourth panel of Fig. 11); this time is plotted as a function of the geometric driving term of Eq. (15). The curve represents the model value of this function evaluated for angle shifts. The errors on the data points are smaller than the symbols; the differences between the data and the curve have been plotted in the lower panel. The tighter group of points in the middle of the plot includes data on position changes. These points also lie along the model curve. The high degree of overlap indicates that for this detection system at forward angles, the effects of an angle change and a position change are similar enough that the corrections can be successfully calculated from a single driving term.

This same information is shown in Fig. 18 for the cross-ratio asymmetry taken with the data from the tensor polarized states. The curve represents the best-fit reproduction to all of the data

Table 3
Rate error parameters (front detector).

Name	Value
Left–right asymmetry	0.0163(6)
Vector coefficient for LR asymmetry	−0.011(3)
Down–up asymmetry	0.0094(6)
Vector coefficient for DU asymmetry	0.00093(15)
Tensor asymmetry	−0.0040(7)
Vector coefficient for tensor asymmetry	−0.0030(11)
Tensor coefficient for tensor asymmetry	−0.002(3)
Horizontal vector beam cross ratio	0.0065(9)
Horizontal tensor beam cross ratio	0.0054(14)
Vertical vector beam cross ratio	−0.0001(8)
Vertical tensor beam cross ratio	−0.0014(12)

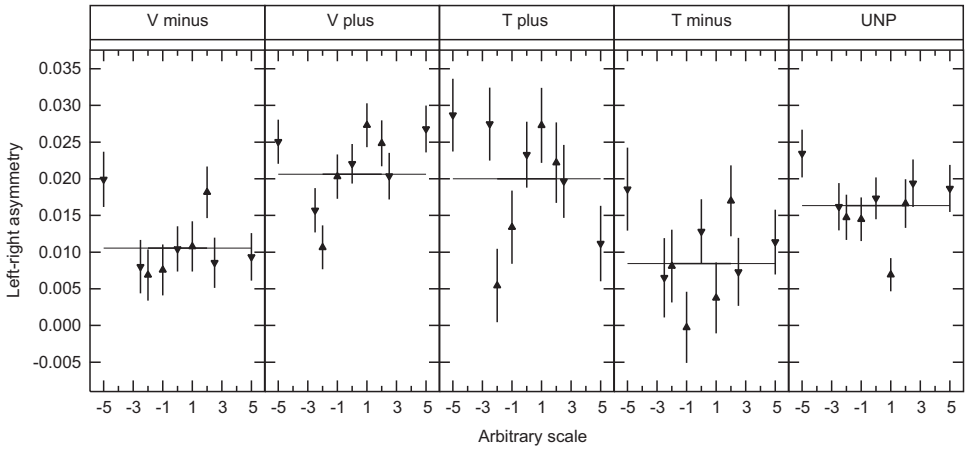

Fig. 16. Like Fig. 11, except that the measurements are for the slope used in the rate correction.

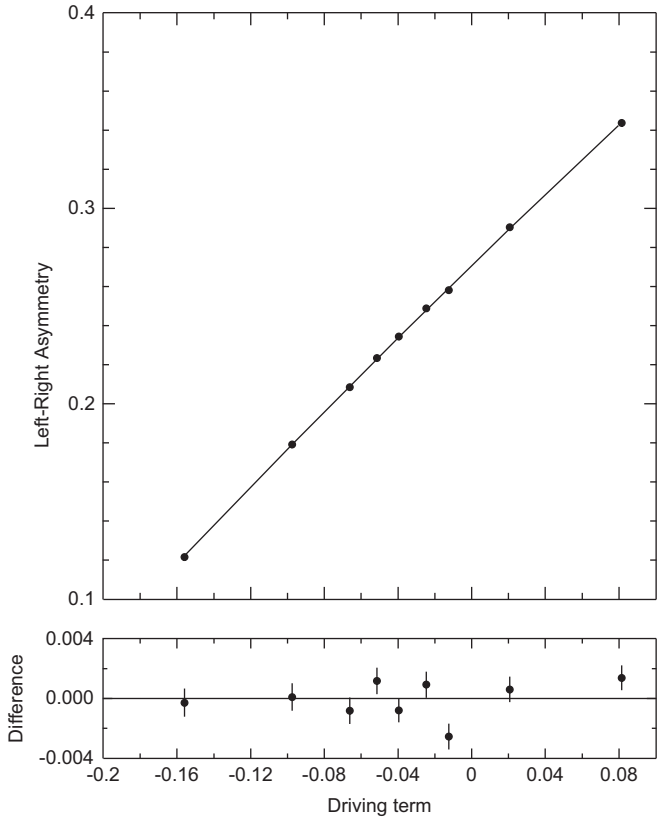

Fig. 17. Measurements of the left–right asymmetry (Eq. (8)) for the T− polarization state and the front detector system plotted as a function of the geometric driving term. Both angle and position changes are included. The five position points are clustered near the center, the five angle points span the plot. The curve is the model value for the dependence of the asymmetry on this driving term. The lower panel shows the differences between the data and the curve.

from the front detector system. It is an adequate representation of both the position and angle measurements from a statistical perspective. In this case the conclusion is unchanged, the single driving term represents an adequate way to determine corrections for either position or angle misalignments.

The formula for the corrected cross-ratio asymmetry now becomes

$$\varepsilon_{CR,corr} = \frac{r-1}{r+1} - \left(\frac{\partial \varepsilon_{CR}}{\partial \phi}\right)_{MODEL} \Delta\phi - \left(\frac{\partial \varepsilon_{CR}}{\partial W}\right)_{MODEL} \Delta W \qquad (18)$$

where r was defined in Eq. (9). The two differences, $\Delta\phi$ and ΔW, are the departures of these driving terms from their values for a nominally aligned and low current beam. The formulas for other polarization observables are similar. The partial derivatives may come from a model such as the one described here, or from a curve such as a polynomial that represents measurements of the observable as a function of the driving term. For larger changes that reach beyond the linear region of the derivatives, each of the two correction terms may be replaced with a more elaborate model or fit of the driving term differences. In either case, once the calibration has been made of the effects of systematic displacements or rate changes, Eq. (18) becomes the "new" cross ratio that can be used in real time to calculate corrected values of the asymmetry.

As a demonstration of how this might operate, Fig. 19 shows the time evolution of a left–right asymmetry during a store. These data were taken with a large, fixed angle shift of the beam on target. The original data points are plotted as open circles. They slope downward because of rate effects in the detectors. By applying the rate correction, the third term in Eq. (18), these points are shifted to the values marked with a cross. This takes

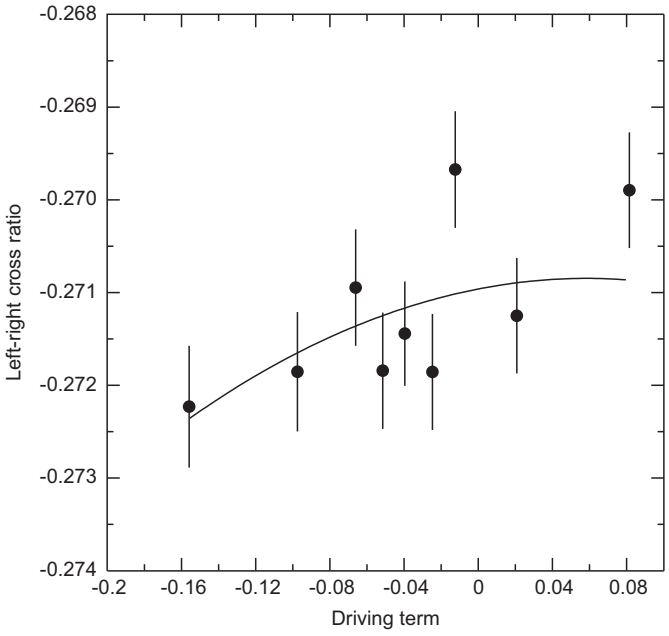

Fig. 18. Like Fig. 17 except that the measurements are the cross-ratio asymmetry.

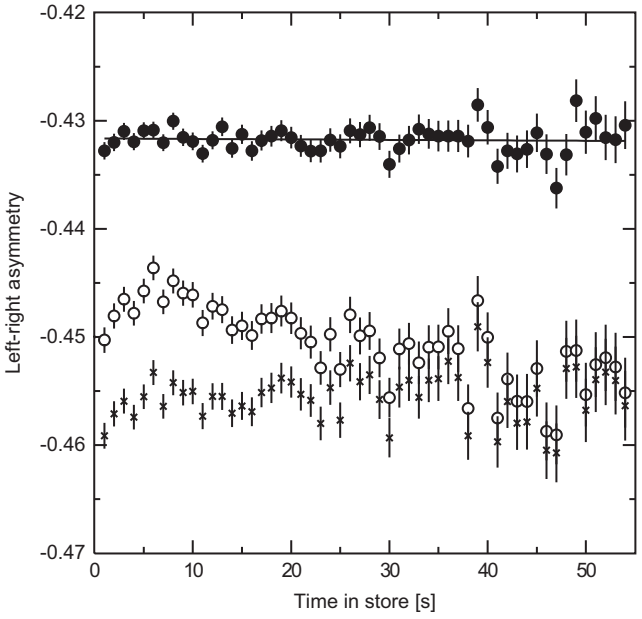

Fig. 19. Measurements of the simple left–right asymmetry as a function of the time in a store. The open circles are the original measurements, the crosses include the correction for rate effects, and the black points the additional correction for geometric effects. See the text for further details.

out much of the variation of the measurements with time. When the geometric correction, the second term in Eq. (18), is applied, the data are moved to the black solid points. A straight line fit through these points with time is shown. The slope of this line is $[-4 \pm 11] \times 10^{-6}\,s^{-1}$. The error in this slope, which is at the level of 10^{-5}, represents the degree to which the procedures described in this paper can be tested using the data available from the COSY experiment.

(The errors for the corrected data points in this illustration are smaller than the errors on the original points. The original data had input from the left and right detector rates for only a single polarization state. The correction for geometry, however, was based on s, which is composed of measurements from two polari-

zation states. In the application of the correction, the correlations between r and s act to both reduce the fluctuations in the corrected data and to make the final statistical error smaller. In the act of correcting, the information from the second polarization state has been incorporated into the final answer. This situation arises only for observables such as the left–right asymmetry. This case was chosen as an illustration of the method because the changes from rate and geometry effects are large and easy to appreciate. For the more usual case of the cross ratio, the changes are considerably smaller.)

For the EDM polarimeter, the actual geometric errors are expected to be much smaller. If one assumes a position error of 0.1 mm and an initial asymmetry of $\varepsilon=0.01$, then the size of the correction calculated from Eq. (10) is approximately 0.3×10^{-6}. The precision with which the correction would be known is likely to be much less than this change. Was the EDDA detector the EDM polarimeter, the goal of keeping errors less than one part per million would be achieved. In optimizing the EDM polarimeter, it is likely that the acceptance will be extended to more forward angles where additional spin-dependence can be included. The cost of this will be larger derivatives, particularly for the cross section. Simple asymmetries will be harder to correct to the required level of precision. At the same time, using the cross ratio avoids, at least at second order, any contribution from derivatives other than those of the analyzing power. Such considerations will be important in making an appropriate optimization of the polarimeter design.

4. Conclusions

Motivated by the goals of creating a polarimeter with high efficiency and of suppressing systematic errors to a level below one part per million, the present study of polarimeter design and systematic error sensitivity was undertaken at the COSY synchrotron in Jülich. The existing EDDA detector was used as a substitute for a future EDM polarimeter, and its operating characteristics were chosen to mimic as much as possible the EDM polarimeter operating point. That point involved the emphasis on deuteron elastic scattering from a carbon target selected by having the elastic deuterons be stopped in the final scintillator. This optimization worked well, producing a configuration with a moderately large analyzing power.

A thick carbon target is needed for the polarimeter to make the efficiency large. In this case, a tube target of 1.5 cm thickness was used, and the beam was extracted along the upper flat edge of the target. The resulting efficiency was in good agreement with a simulation based on measured deuteron scattering and reaction cross sections. This supports confidence in other designs for an EDM polarimeter that show efficiencies approaching 1%.

The main effort of the experiment was to study the effects of geometric and rate-induced changes on the measured polarization observables, and in particular on the cross ratio. The changes used in the experiment were deliberately much larger than those expected in a real experiment. This made these effects easily accessible for measurement. An initial study at the KVI revealed that parameterizations such as the cross ratio have substantial second-order systematic errors despite canceling effects at first order. A large data set was accumulated at COSY and represented by a model of polarization effects and systematic errors that successfully reproduced all features of the data. Based on this study, it was possible to define correction driving terms for geometry and rate, and to explain all observed systematic errors in terms of these two parameters. The quality of the result was enhanced because the forward angle nature of the detectors rendered position and angle error effects very similar in the polarimeter data. For observables such as the cross ratio, it appears that under the level of control expected in an EDM search, the corrections to the cross ratio and especially the precision with which they will be known is comfortably less than one part per million. Once calibrated, these corrections can be applied in real time to generate asymmetries that would be useful for feedback purposes in an EDM search.

Acknowledgements

The authors wish to thank the staffs of the KVI and COSY for their support during these experimental efforts. Special thanks go to Frank Hinterberger who helped with the understanding of the EDDA detector and to the SPIN@COSY Collaboration who allowed us to participate in a COSY run prior to the beginning of these efforts. Financial support is acknowledged through NSF Grants PHY-0457219 and PHY-0758018, an Innovational Research Grant and a Toptalent Grant by the Dutch Foundation for Scientific Research (NWO), and the Helmholtz Association through funds provided to the virtual institute "Spin and strong QCD" (VH-VI-231) and JCHP/Jülich Center of Hadron Physics. This publication has been supported by the European Commission under the 7th Framework Program through the 'Research Infrastructures' action of the 'Capacities' Programme. The call is FP7-INFRASTRUCTURES-2008-1, Grant Agreement N. 227431.

This manuscript has been authorized by the Brookhaven Science Associates, LLC under Contract no. DE-AC02-98CH1-886 with the U.S. Department of Energy. The United States Government retains, and the publisher, by accepting the article for publication, acknowledges, a world-wide license to publish or reproduce the published form of this manuscript, or allow others to do so, for the United States Government purposes.

References

[1] F.J.M. Farley, K. Jungmann, J.P. Miller, W.M. Morse, Y.F. Orlov, B.L. Roberts, Y.K. Semertzidis, A. Silenko, E.J. Stephenson, Physical Review Letters 93 (2004) 052001.
[2] G.G. Ohlsen, P.W. Keaton Jr., Nuclear Instruments and Methods 109 (1973) 41.
[3] R. Maier, Nuclear Instruments and Methods A 390 (1997) 1.
[4] S. Brandenburg (AGOR Construction Group), in: E.R. Lindstrom, L.S. Taylor (Eds.), in: Proceedings of the 1987 IEEE Particle Accelerator Conference, 1987, IEEE, New York, p. 376.
[5] R. Bieber, et al., Nuclear Instruments and Methods A 457 (2001) 12.
[6] K. Sekiguchi, et al., Physical Review C 65 (2002) 034003.
[7] H. Witała, et al., Few-Body Systems 15 (1993) 67.
[8] M. Garçon, et al., Nuclear Physics A 458 (1986) 287.
[9] K. Hatanaka, et al., Nuclear Physics A 426 (1984) 77.
[10] A.M. van den Berg, et al., Nuclear Instruments and Methods B 99 (1995) 637.
[11] V.P. Ladygin, et al., Nuclear Instruments and Methods A 404 (1998) 129.
[12] B. Bonin, et al., Nuclear Instruments and Methods A 288 (1990) 389.
[13] D. Albers, et al., European Physical Journal A 22 (2004) 125.
[14] J. Bisplinghoff, et al., Nuclear Instruments and Methods A 329 (1993) 151.
[15] P.D. Eversheim, et al., AIP Conference Proceedings (AIP, Woodbury, NY) 339 (1995) 668;
R. Weidmann, et al., Review of Scientific Instruments 67 (1996) 1357.
[16] A. Lehrach, et al., AIP Conference Proceedings 675 (2003) 153.
[17] Pierre Marmier, Eric Sheldon, Physics of Nuclei and Particles, Academic Press, New York, 1969–70.
[18] Joseph F. Janni, Atomic Data and Nuclear Data Tables 27 (1982) 147;
Joseph F. Janni, Atomic Data and Nuclear Data Tables 27 (1982) 341.
[19] H. Okamura, et al., Physical Review C 58 (1998) 2180.
[20] C. Bäumer, et al., Physical Review C 63 (2001) 037601.
[21] T. Kawabata, et al., Physical Review C 70 (2004) 034318.
[22] Y. Satou, et al., Physics Letters B 549 (2002) 307.
[23] Philip R. Bevington, Data Reduction and Error Analysis for the Physical Sciences, third ed., McGraw-Hill, Boston, 2003.